

## Electrochemical Properties of Spherical Hollow Composite Powders with Various $\text{Li}_4\text{Ti}_5\text{O}_{12}/\text{SnO}_2$ Ratios Prepared by Spray Pyrolysis

Kwang Min Yang<sup>1</sup>, Yun Chan Kang<sup>1,\*</sup>, Sang Mun Jeong<sup>2</sup>, Yun Ju Choi<sup>3</sup>, Yang Soo Kim<sup>3</sup>

<sup>1</sup> Department of Chemical Engineering, Konkuk University, 1 Hwayang-dong, Gwangjin-gu, Seoul 143-701, Republic of Korea

<sup>2</sup> Department of Chemical Engineering, Chungbuk National University, Cheongju, Chungbuk 361-763, Republic of Korea

<sup>3</sup> Suncheon Center, Korea Basic Science Institute, Suncheon 540-742, Republic of Korea

\*E-mail: [yckang@konkuk.ac.kr](mailto:yckang@konkuk.ac.kr)

Received: 19 May 2013 / Accepted: 27 August 2013 / Published: 10 September 2013

---

$\text{Li}_4\text{Ti}_5\text{O}_{12}$ - $\text{SnO}_2$  composite powders with different  $\text{Li}_4\text{Ti}_5\text{O}_{12}/\text{SnO}_2$  ratios and comprising hollow and sphere particles are prepared by an ultrasonic spray pyrolysis process. The composite powders exhibit mixed-crystal structures consisting of  $\text{Li}_4\text{Ti}_5\text{O}_{12}$  and  $\text{SnO}_2$  phases with no impurities being present, irrespective of their  $\text{Li}_4\text{Ti}_5\text{O}_{12}/\text{SnO}_2$  ratios. The composite powders with low concentrations of  $\text{SnO}_2$  contained  $\text{SnO}_2$  nanocrystals several tens of nanometers in size, which are uniformly distributed in the  $\text{Li}_4\text{Ti}_5\text{O}_{12}$  matrix. Complete necking between the  $\text{SnO}_2$  nanocrystals results in an increase in the electrical conductivity of the composite powder with a high concentration of  $\text{SnO}_2$  ( $\text{Li}_4\text{Ti}_5\text{O}_{12}/\text{SnO}_2 = 0.4/0.6$ ). These composite powders exhibit a high initial charge capacity of  $730 \text{ mAh g}^{-1}$  and good cyclability even at a high charge-and-discharge rate of  $700 \text{ mA g}^{-1}$  for voltages between 0.1 and 2.5 V. In addition, it retained 70% of its initial capacity after 60 cycles. The initial charge capacities of this composite powder are 572, 399, and  $303 \text{ mAh g}^{-1}$  at the extremely high charge-and-discharge rates of 3500, 7000, and  $14000 \text{ mA g}^{-1}$ , respectively.

---

**Keywords:** lithium titanate; tin oxide; spray pyrolysis; composite powders; electrochemical properties

### 1. INTRODUCTION

$\text{Li}_4\text{Ti}_5\text{O}_{12}$ - and  $\text{SnO}_2$ -based composite materials have been studied with the aim of obtaining anodic materials with high capacities and good cyclabilities for use in lithium-ion batteries [1-9].  $\text{Li}_4\text{Ti}_5\text{O}_{12}$ -based composite powders with improved electrochemical properties have been developed by

enhancing the electronic conductivity of  $\text{Li}_4\text{Ti}_5\text{O}_{12}$ . However,  $\text{Li}_4\text{Ti}_5\text{O}_{12}$  has a relatively low theoretical capacity ( $175 \text{ mAh g}^{-1}$ ).  $\text{SnO}_2$ -based materials have also been studied widely to devise methods of retarding the large changes (of up to 300%) that take place in the volume of  $\text{SnO}_2$  during the insertion or removal of  $\text{Li}^+$  ions when used in lithium-ion batteries. The inactive or active component that does not undergo volume change during cycling buffers the large change in the volume of  $\text{SnO}_2$ , which has a high theoretical capacity ( $781 \text{ mAh g}^{-1}$ ) [6-12]. A  $\text{Li}_4\text{Ti}_5\text{O}_{12}$ - $\text{SnO}_2$  composite with a controlled morphology could overcome the disadvantages associated with the two anodic materials. The electrochemical properties of  $\text{Li}_4\text{Ti}_5\text{O}_{12}$ - $\text{SnO}_2$  (or Sn) composite powders prepared by high-energy mechanical milling, sol-gel, and solution precipitation have been reported [13-16]. In the previous studies,  $\text{Li}_4\text{Ti}_5\text{O}_{12}$  or  $\text{SnO}_2$  powders had to be used as colloidal seed materials to fabricate the composite powders. The characteristics of these powders, such as the distribution of each phase, phase homogeneity, mean size, and internal structure, among others, affected the electrochemical properties of the composite anodic materials strongly. Therefore, the development of an appropriate process for preparing such composite powders is one of the major challenges in improving lithium-ion batteries.

Spray pyrolysis had been reported to be suitable for the large-scale and continuous production of multicomponent cathodic and anodic materials for lithium-ion batteries [17-20]. Spray pyrolysis is also suitable for the preparation of composite powders comprising two different phases, because of the microscaled reactions involving each component that take place within the micron-sized droplets [20-23].

In this study, composite powders with different  $\text{Li}_4\text{Ti}_5\text{O}_{12}/\text{SnO}_2$  ratios and comprising spherical and hollow particles were prepared by an ultrasonic spray process using an aqueous spray solution. The morphologies, crystal structures, and electrochemical properties of the composite powders, which had both high and low concentrations of  $\text{SnO}_2$ , were investigated.

## 2. EXPERIMENTAL

The precursor powders for the  $\text{Li}_4\text{Ti}_5\text{O}_{12}$ - $\text{SnO}_2$  composite powders were prepared by ultrasonic spray pyrolysis. The equipment used for the preparation consisted of six ultrasonic spray generators operated at 1.7 MHz, a tubular quartz reactor (length = 1000 mm; inner diameter = 50 mm), and a bag filter. The spray pyrolysis process was performed at a fixed temperature of  $900^\circ\text{C}$ . The flow rate of air, which was used as the carrier gas during the process, was fixed at  $10 \text{ Lmin}^{-1}$ . The spray solution used was prepared by dissolving appropriate amounts of lithium nitrate ( $\text{LiNO}_3$ ; Aldrich), titanium tetraisopropoxide (TTIP) ( $\text{Ti}(\text{OCH}(\text{CH}_3)_2)_4$ ; Junsei) and tin oxalate ( $\text{SnC}_2\text{O}_4$ ; Aldrich) in distilled water containing an appropriate amount of nitric acid. The amount of lithium nitrate added to the spray solution was in excess of 5 wt% of the stoichiometric amount required to facilitate the formation of a  $\text{Li}_4\text{Ti}_5\text{O}_{12}$  phase. The overall concentration of the Li, Ti, and Sn components was 0.5 M. Citric acid with a concentration of 0.5 M was used as the chelating agent. The precursor powders obtained using the spray pyrolysis process were heat treated at a temperature of  $800^\circ\text{C}$  for 3 h in air to obtain the composite powders.

The crystal structures of the composite powders obtained after the heat treatment were investigated using X-ray diffraction (XRD) analysis (Rigaku DMAX-33), performed at the Korea Basic Science Institute (Daegu). The morphological characteristics of the powders were investigated using scanning electron microscopy (SEM) (JEOL JSM-6060) and transmission electron microscopy (TEM) (JEOL JEM-2010). The surface areas of the powders were measured by employing the Brunauer–Emmett–Teller (BET) method with  $N_2$  as adsorbate gas.

The capacities and cyclabilities of the  $Li_4Ti_5O_{12}$ - $SnO_2$  composite powders were measured using 2032-type coin cells. Electrodes were made from 40 mg samples of the composite powders, which were mixed with 5 mg of carbon black and 5 mg of sodium carboxymethyl cellulose (CMC) in distilled water. Li metal and a polypropylene film were used as the counter electrode and separator, respectively.  $LiPF_6$  (1 M) in a mixture of ethylene carbonate (EC) and dimethyl carbonate (DMC) in a 1:1 volume ratio, with 2 wt% vinylene carbonate (VC) added to the mixture, was used as the electrolyte (Techno Semichem. Co.). The cells were assembled in a glove box in an argon atmosphere. The electrochemical properties of the composite powders were measured via cycling using voltages of 0.1–2.5 V at various current densities.

### 3. RESULTS AND DISCUSSIONS

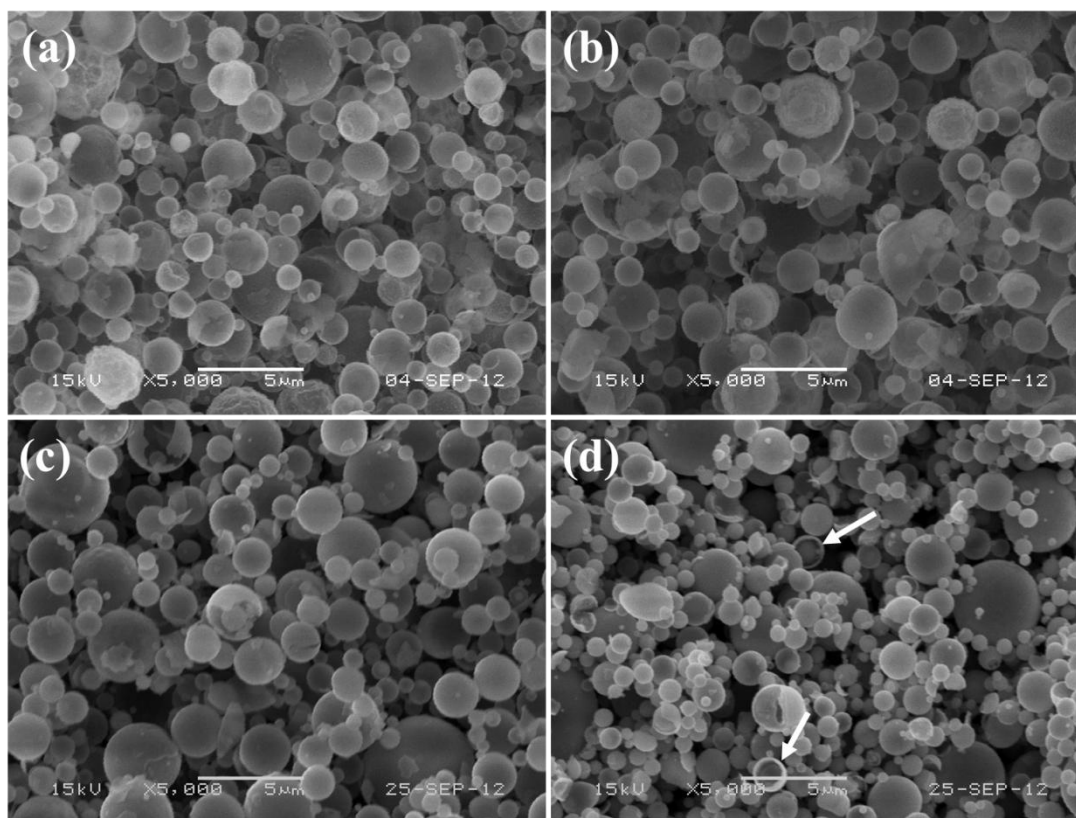


**Figure 1.** SEM images of the precursor powders with different  $Li_4Ti_5O_{12}/SnO_2$  ratios prepared directly by spray pyrolysis: (a) 0.8/0.2, (b) 0.6/0.4, (c) 0.4/0.6, (d) 0.2/0.8.

The morphologies of the precursor powders with different  $\text{Li}_4\text{Ti}_5\text{O}_{12}/\text{SnO}_2$  ratios, prepared directly by spray pyrolysis, are shown in Fig. 1. The particles of the precursor powders were micron sized, spherical, and hollow, irrespective of their compositions. The particles of the pure  $\text{Li}_4\text{Ti}_5\text{O}_{12}$  and  $\text{SnO}_2$  powders (not shown in this manuscript), prepared via spray pyrolysis using a citric acid-free aqueous spray solution, were fine sized and had spherical shapes and dense structures. Each droplet usually results in the formation of a single dense particle—via densification—during the preparation of the powders. However, in this study, each droplet resulted in the formation of a hollow powder particle during the spray pyrolysis process. Citric acid, used as the chelating agent, changed the drying and decomposition characteristics of the metal salts. In addition, the abrupt evolution of gas owing to the decomposition of the metal chelates resulted in the formation of precursor powders with particles that were hollow in shape and large in size.

The precursor powders prepared directly via spray pyrolysis exhibited poor electrochemical properties. This was because the powders were present within the hot-walled reactor, maintained at  $900^\circ\text{C}$ , for only a short period (7 s). This is also the reason the precursor powders had to be heat treated at  $800^\circ\text{C}$  to form the  $\text{Li}_4\text{Ti}_5\text{O}_{12}\text{-SnO}_2$  composite powders.

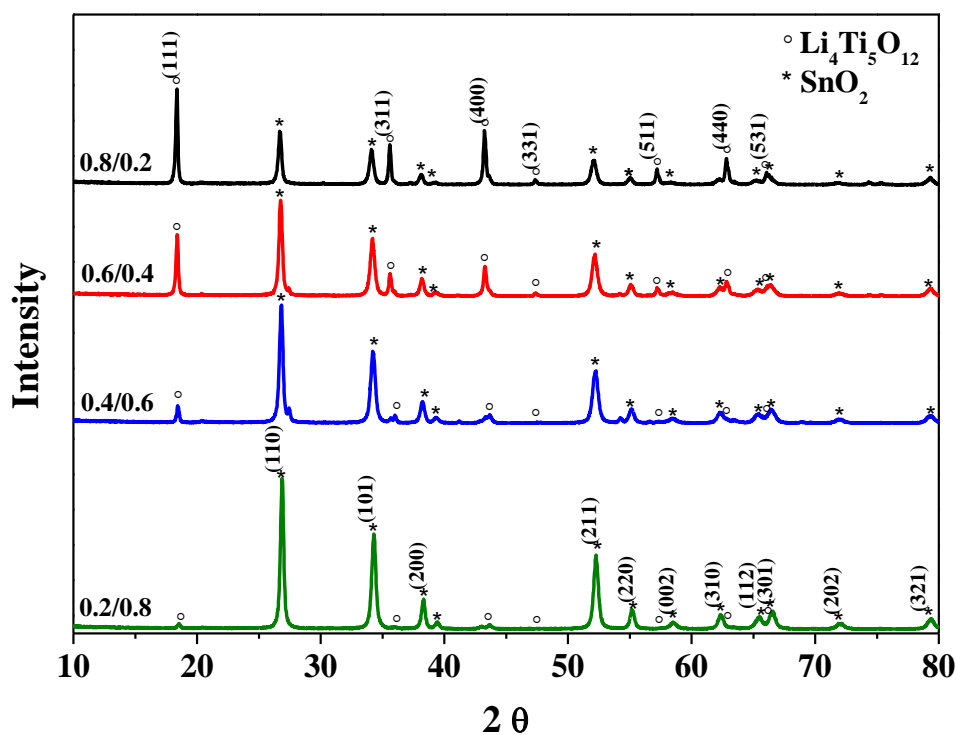


**Figure 2.** XRD patterns of the composite powders with different  $\text{Li}_4\text{Ti}_5\text{O}_{12}/\text{SnO}_2$  ratios post-treated at  $800^\circ\text{C}$ .

Fig. 2 shows the crystal structures of the heat-treated composite powders with different  $\text{Li}_4\text{Ti}_5\text{O}_{12}/\text{SnO}_2$  ratios. The diffraction patterns of the composite powder with a high concentration of  $\text{SnO}_2$  ( $\text{Li}_4\text{Ti}_5\text{O}_{12}/\text{SnO}_2 = 0.2/0.8$ ) mainly contained peaks attributable to  $\text{SnO}_2$ , with smaller peaks ascribable to  $\text{Li}_4\text{Ti}_5\text{O}_{12}$  also being present. The intensity of the peaks related to the  $\text{Li}_4\text{Ti}_5\text{O}_{12}$  phase increased with an increase in the  $\text{Li}_4\text{Ti}_5\text{O}_{12}/\text{SnO}_2$  ratio. Consequently, the diffraction patterns of the

composite powder with a low concentration of SnO<sub>2</sub> (Li<sub>4</sub>Ti<sub>5</sub>O<sub>12</sub>/SnO<sub>2</sub> = 0.8/0.2) contained primary peaks related to both the Li<sub>4</sub>Ti<sub>5</sub>O<sub>12</sub> phase and the SnO<sub>2</sub> phase. The diffraction patterns of all the composite powders contained peaks related to the Li<sub>4</sub>Ti<sub>5</sub>O<sub>12</sub> and SnO<sub>2</sub> phases alone, with no peaks attributable to any impurities being present. This was the case irrespective of the Li<sub>4</sub>Ti<sub>5</sub>O<sub>12</sub>/SnO<sub>2</sub> ratios. The mean size of the SnO<sub>2</sub> crystallites, measured from the peak widths of (110) peaks using the Scherrer's equation, was 27 nm, irrespective of the Li<sub>4</sub>Ti<sub>5</sub>O<sub>12</sub>/SnO<sub>2</sub> ratio.

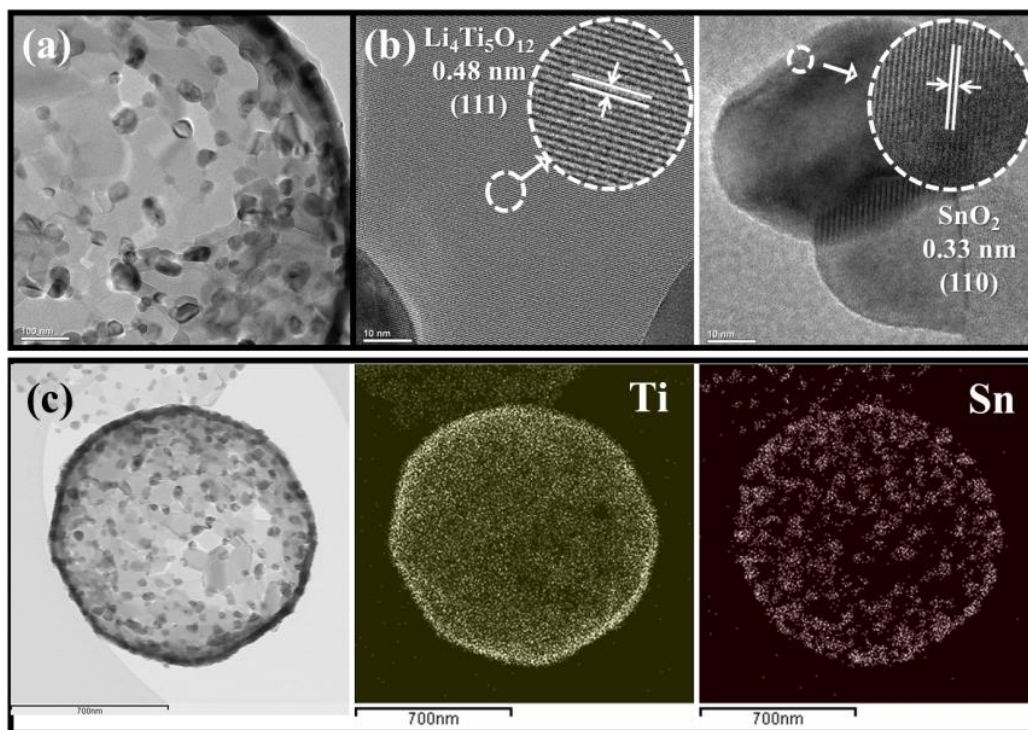


**Figure 3.** TEM and dot-mapping images of the post-treated Li<sub>4</sub>Ti<sub>5</sub>O<sub>12</sub>-SnO<sub>2</sub> (0.8/0.2) composite powders.

The TEM and dot-mapping images of the composite powders with different Li<sub>4</sub>Ti<sub>5</sub>O<sub>12</sub>/SnO<sub>2</sub> ratios are shown in Figs. 3–6. The particles of the composite powders had a spherical shape and a hollow structure, even after the heat treatment at 800°C, irrespective of the Li<sub>4</sub>Ti<sub>5</sub>O<sub>12</sub>/SnO<sub>2</sub> ratio. The TEM and dot-mapping images of the composite powders suggested the presence of two separate phases. In the composite powder with a low concentration of SnO<sub>2</sub> (Li<sub>4</sub>Ti<sub>5</sub>O<sub>12</sub>/SnO<sub>2</sub> = 0.8/0.2), shown in Fig. 3, the Li<sub>4</sub>Ti<sub>5</sub>O<sub>12</sub> and SnO<sub>2</sub> phases were observably distinct. High-resolution TEM images of the composite powders, shown in Fig. 3b, showed clear lattice fringes separated by 0.48 and 0.33 nm. These values correspond to the (111) plane of Li<sub>4</sub>Ti<sub>5</sub>O<sub>12</sub> and the (110) plane of SnO<sub>2</sub>, respectively. The results of the dot mapping of the composite powders, shown in Fig. 3c, also indicated that the dark nanocrystals seen in the TEM images were of SnO<sub>2</sub>. SnO<sub>2</sub> nanocrystals several tens of nanometers in size were uniformly distributed in the Li<sub>4</sub>Ti<sub>5</sub>O<sub>12</sub> matrix, as can be seen from the TEM image in Fig. 3a. The mean size of the SnO<sub>2</sub> crystallites measured from the TEM image was similar to that calculated using the Scherrer's equation and the peak widths of the XRD patterns. Therefore, it was concluded

that the  $\text{SnO}_2$  nanocrystals seen in the TEM images in Fig. 3 were single crystals. In the case of the composite powders with reversed ratios of  $\text{Li}_4\text{Ti}_5\text{O}_{12}$  and  $\text{SnO}_2$  ( $\text{Li}_4\text{Ti}_5\text{O}_{12}/\text{SnO}_2 = 0.6/0.4$  and  $0.4/0.6$ ), shown in Figs. 4 and 5, respectively, a clear separation of the  $\text{Li}_4\text{Ti}_5\text{O}_{12}$  and  $\text{SnO}_2$  phases was observed in the corresponding high-resolution TEM and dot-mapping images.

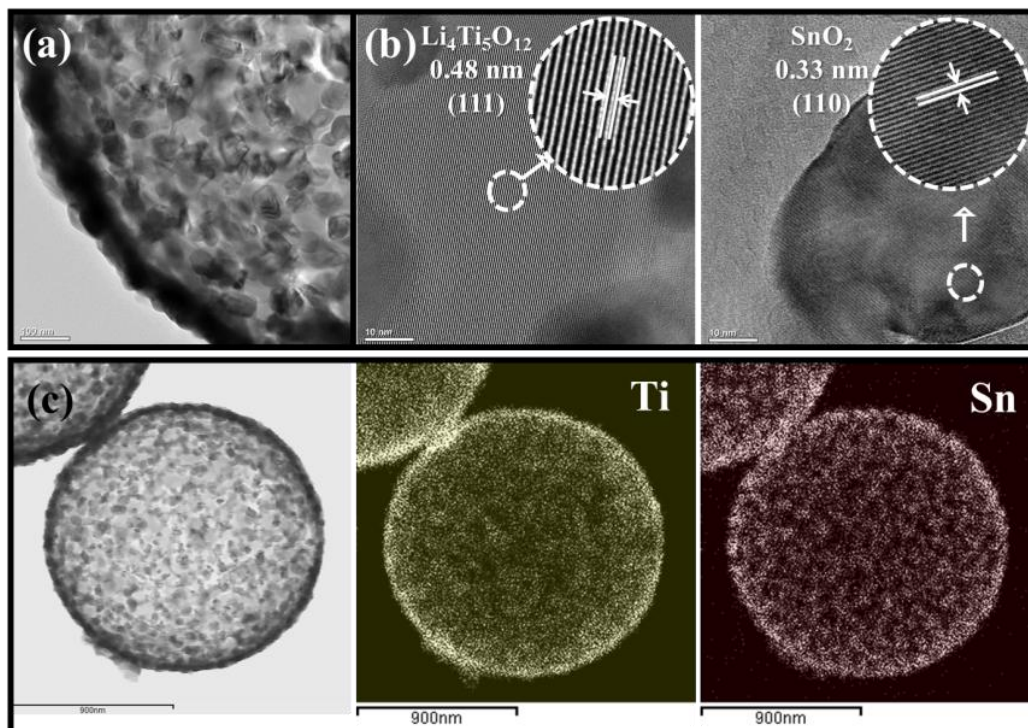


**Figure 4.** TEM and dot-mapping images of the post-treated  $\text{Li}_4\text{Ti}_5\text{O}_{12}$ - $\text{SnO}_2$  (0.6/0.4) composite powders.

The mean sizes of the  $\text{SnO}_2$  crystallites, measured using the TEM images shown in Figs. 3–5, were 32, 49, and 66 nm, respectively, with the size of the  $\text{SnO}_2$  crystals increasing with an increase in the  $\text{SnO}_2$  concentration. Necking between the  $\text{SnO}_2$  nanocrystals were not observed in the TEM image shown in Fig. 3a. However, complete necking between the  $\text{SnO}_2$  nanocrystals, which resulted in the crystals being highly electrically conductive, was seen in the TEM images shown in Fig. 5a. As can be seen from the figure, the  $\text{Li}_4\text{Ti}_5\text{O}_{12}$  nanocrystals were surrounded by a network of  $\text{SnO}_2$  nanocrystals. In the composite powder with a high concentration of  $\text{SnO}_2$  ( $\text{Li}_4\text{Ti}_5\text{O}_{12}/\text{SnO}_2 = 0.2/0.8$ ), a clear separation of the phases of the composite powder were not observed in the corresponding TEM image, shown in Fig. 6. It was noticed from the dot-mapping images, shown in Fig. 6c, that the Ti component, which originated from the  $\text{Li}_4\text{Ti}_5\text{O}_{12}$  nanocrystals, was uniformly distributed in the composite powders. Therefore, it was assumed that  $\text{Li}_4\text{Ti}_5\text{O}_{12}$  nanocrystals few nanometers in size would also be uniformly distributed in the  $\text{SnO}_2$  crystal matrix. In keeping in this assumption, well-defined peaks ascribable to the  $\text{Li}_4\text{Ti}_5\text{O}_{12}$  phase of the composite powder with a  $\text{Li}_4\text{Ti}_5\text{O}_{12}/\text{SnO}_2$  ratio of 0.2/0.8 were not observed in the corresponding XRD patterns, as can be seen from Fig. 2. The TEM image of this composite powder, which can be seen in Fig. 6a, was more filled out than those of the other powders, shown in

Figs. 3–5. This was because this composite powder ( $\text{Li}_4\text{Ti}_5\text{O}_{12}/\text{SnO}_2 = 0.2/0.8$ ), which contained  $\text{SnO}_2$  in a high concentration, had a yolk-shell structure.

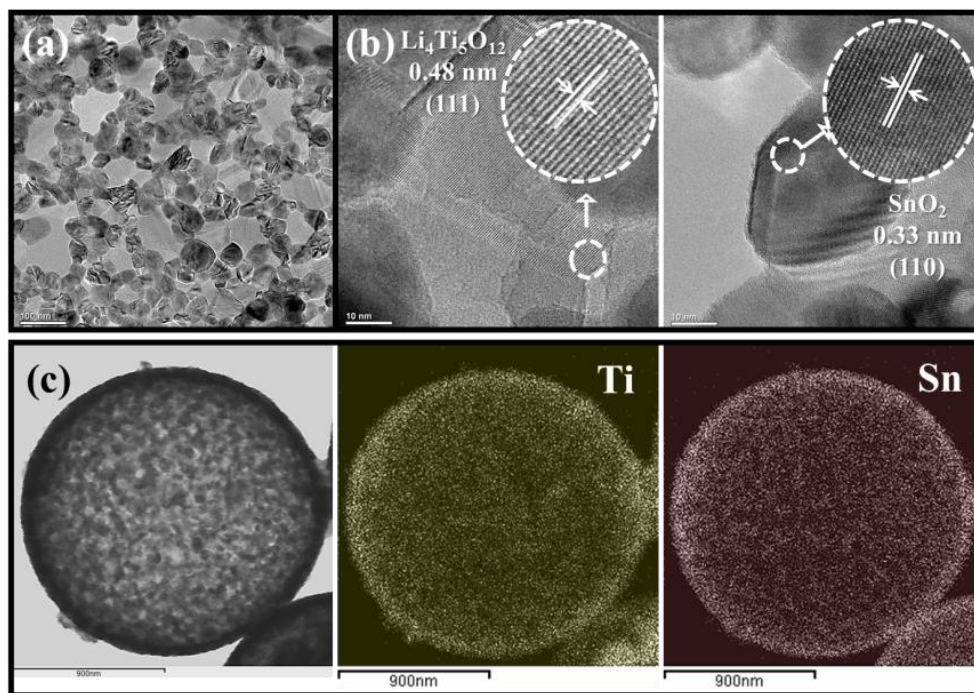


**Figure 5.** TEM and dot-mapping images of the post-treated  $\text{Li}_4\text{Ti}_5\text{O}_{12}\text{-SnO}_2$  (0.4/0.6) composite powders.

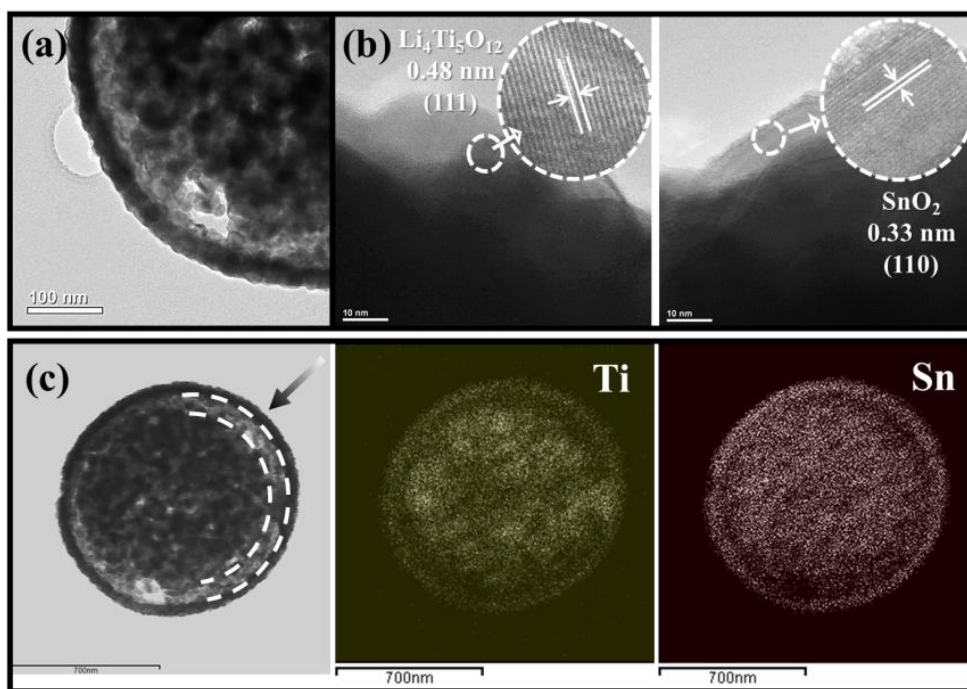


**Figure 6.** TEM and dot-mapping images of the post-treated  $\text{Li}_4\text{Ti}_5\text{O}_{12}\text{-SnO}_2$  (0.2/0.8) composite powders.

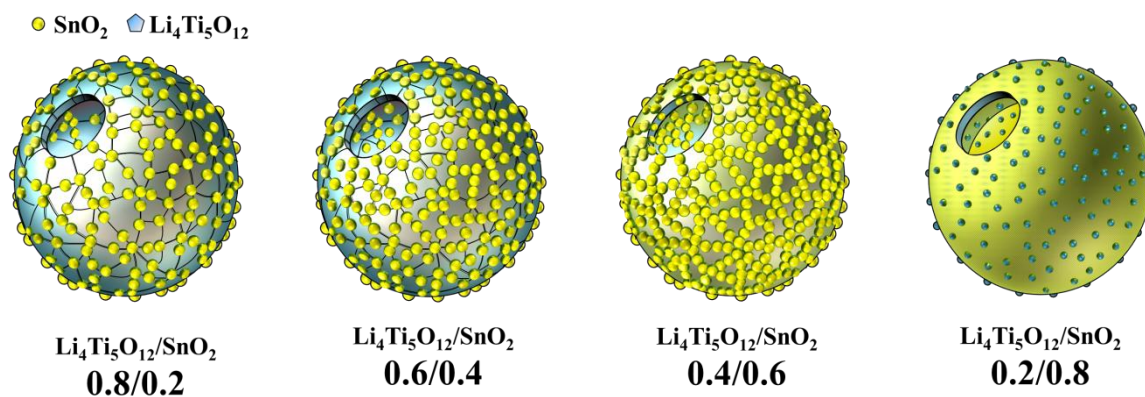


**Figure 7.** Schematic diagram of the structure of the composite powders with different Li<sub>4</sub>Ti<sub>5</sub>O<sub>12</sub>/SnO<sub>2</sub> ratios.

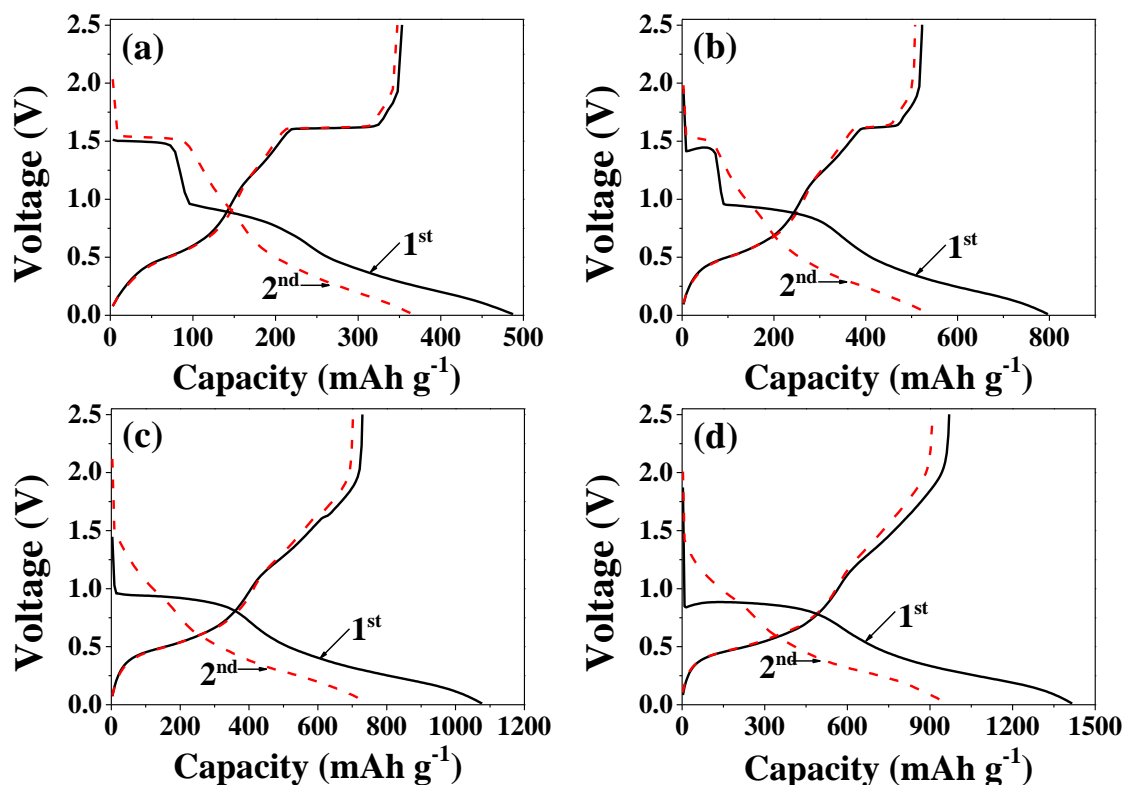
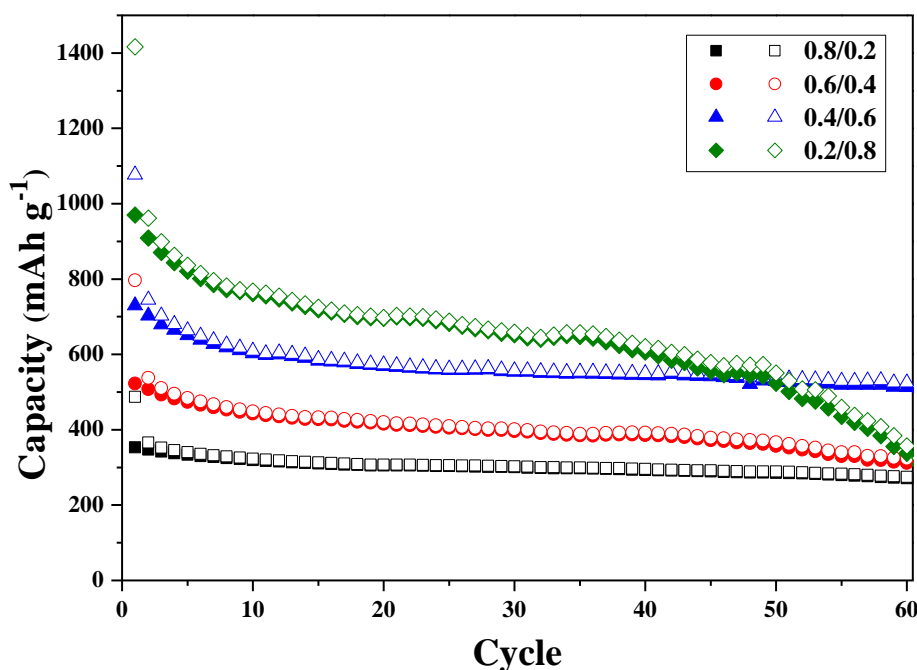


**Figure 8.** Charge and discharge curves of the composite powders with different Li<sub>4</sub>Ti<sub>5</sub>O<sub>12</sub>/SnO<sub>2</sub> ratios: (a) 0.8/0.2, (b) 0.6/0.4, (c) 0.4/0.6, (d) 0.2/0.8.

A clear void space was noticed between the core and the shell parts of the yolk-shell structure in the TEM image of the composite powder, as indicated by the arrow in Fig. 6c. The core part was also observed in the SEM image (Fig. 1d) of the powder, which contained disjointed particles, and is again indicated by arrows. The BET surface areas of the composite powders with Li<sub>4</sub>Ti<sub>5</sub>O<sub>12</sub>/SnO<sub>2</sub> ratios of 0.2/0.8, 0.4/0.6, 0.6/0.4, and 0.8/0.2 were 1.5, 4.2, 8.0, and 8.1 m<sup>2</sup> g<sup>-1</sup>, respectively. Fig. 7

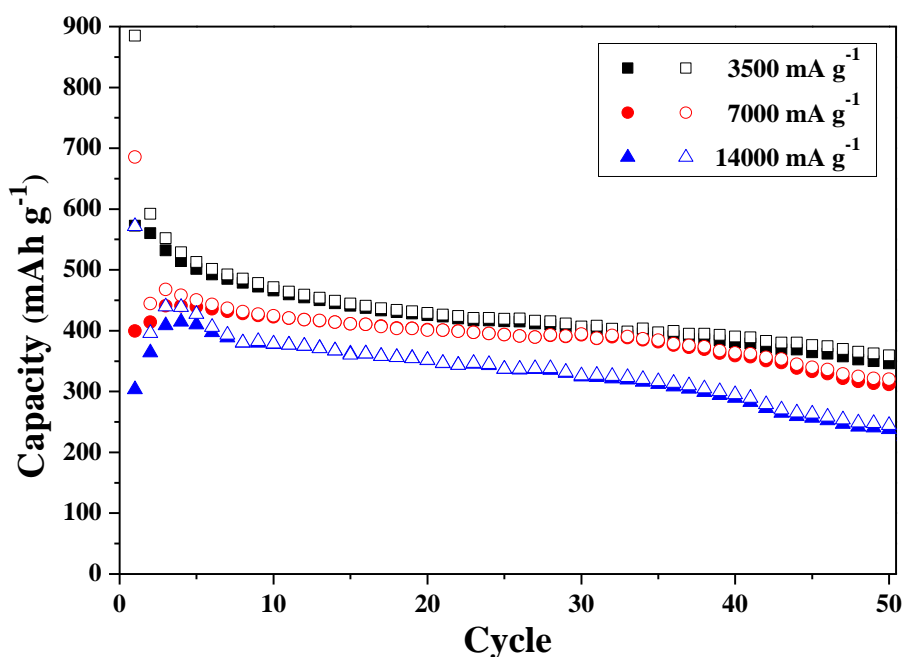
shows schematic diagrams of the structures of the  $\text{Li}_4\text{Ti}_5\text{O}_{12}$ - $\text{SnO}_2$  composite powders prepared by the spray pyrolysis process.

Fig. 8 shows the charge-and-discharge curves for the first and second cycles of the  $\text{Li}_4\text{Ti}_5\text{O}_{12}$ - $\text{SnO}_2$  composite powders with different  $\text{Li}_4\text{Ti}_5\text{O}_{12}/\text{SnO}_2$  ratios, measured at room temperature at a constant charge-and-discharge rate of  $700 \text{ mA g}^{-1}$  for voltages between 0.1 and 2.5 V. The discharge curves for the composite powders with low concentrations of  $\text{SnO}_2$  ( $\text{Li}_4\text{Ti}_5\text{O}_{12}/\text{SnO}_2 = 0.8/0.2$  and  $0.6/0.4$ ) exhibited two distinct potential plateaus, at  $\sim 1.5 \text{ V}$  and at  $\sim 0.8 \text{ V}$ , during their first cycles. The two plateaus could be attributed to the reduction of Ti(IV) to Ti(III) and of Sn(IV) to Sn(0), respectively [24-27]. However, the potential plateaus at  $\sim 1.5 \text{ V}$  were not observed in the first discharge curves of the composite powders with high concentrations of  $\text{SnO}_2$  ( $\text{Li}_4\text{Ti}_5\text{O}_{12}/\text{SnO}_2 = 0.4/0.6$  and  $0.2/0.8$ ). This was because of the high charge-and-discharge rate ( $700 \text{ mA g}^{-1}$ ). The potential plateaus at  $\sim 1.6 \text{ V}$ , attributable to  $\text{Li}_4\text{Ti}_5\text{O}_{12}$  nanocrystals, were also observed in the first and second charge curves of the composite powders with low concentrations of  $\text{SnO}_2$  ( $\text{Li}_4\text{Ti}_5\text{O}_{12}/\text{SnO}_2 = 0.8/0.2$  and  $0.6/0.4$ ). The initial charge-and-discharge capacities of the composite powders increased with a decrease in the  $\text{Li}_4\text{Ti}_5\text{O}_{12}/\text{SnO}_2$  ratio. This was because increasing the concentration of  $\text{SnO}_2$  increased the theoretical capacity of the composite powders. The first Coulombic efficiencies of the composite powders decreased from 73 to 69% when the  $\text{Li}_4\text{Ti}_5\text{O}_{12}/\text{SnO}_2$  ratio was decreased from  $0.8/0.2$  to  $0.2/0.8$ . These large irreversible losses in the capacities of the composite powders were mainly attributable to the formation of  $\text{Li}_2\text{O}$  during the first charging cycle, owing to a reaction of  $\text{SnO}_2$  with Li [28-30]. The lengths of the potential plateaus at  $\sim 1.6$  and  $\sim 1.5 \text{ V}$  in the second charge-and-discharge curves of the composite powders with low concentrations of  $\text{SnO}_2$  did not decrease. This was so because of the high stability of the  $\text{Li}_4\text{Ti}_5\text{O}_{12}$  phase. The decrease in the capacities of the composite powders in the second cycles resulted from the instability of the  $\text{SnO}_2$  component.



**Figure 9.** Cycling properties of the composite powders with different  $\text{Li}_4\text{Ti}_5\text{O}_{12}/\text{SnO}_2$  ratios.

Fig. 9 shows the cyclabilities of the composite powders with different  $\text{Li}_4\text{Ti}_5\text{O}_{12}/\text{SnO}_2$  ratios at a constant charge-and-discharge rate of  $700 \text{ mA g}^{-1}$ . The charge capacities of the composite powder with a high concentration of  $\text{SnO}_2$  ( $\text{Li}_4\text{Ti}_5\text{O}_{12}/\text{SnO}_2 = 0.2/0.8$ ) decreased abruptly from  $970$  to  $338 \text{ mAh g}^{-1}$  after 60 cycles. However, the charge capacities of the composite powders with  $\text{Li}_4\text{Ti}_5\text{O}_{12}/\text{SnO}_2$  ratios of  $0.4/0.6$ ,  $0.6/0.4$ , and  $0.8/0.2$  were high at  $513$ ,  $312$ , and  $271 \text{ mAh g}^{-1}$ , respectively, after 60 cycles. The composite powders with high concentrations of  $\text{Li}_4\text{Ti}_5\text{O}_{12}$  had higher capacities and better cyclabilities even at a high charge-and-discharge rate of  $700 \text{ mA g}^{-1}$ . In particular, the composite powder with a  $\text{Li}_4\text{Ti}_5\text{O}_{12}/\text{SnO}_2$  ratio of  $0.4/0.6$  exhibited a high initial charge capacity of  $730 \text{ mAh g}^{-1}$  and good cyclability even at a high charge-and-discharge rate of  $700 \text{ mA g}^{-1}$ . In addition, the powder was able to retain 70% of its initial capacity after 60 cycles. The uniform mixing of the  $\text{Li}_4\text{Ti}_5\text{O}_{12}$  and  $\text{SnO}_2$  phases, as well as the phase purities, and unique morphologies of the spherical and hollow particles, improved the electrochemical properties of the composite powders prepared by spray pyrolysis. In addition, the complete necking of the  $\text{SnO}_2$  nanocrystals, which resulted in an increase in electrical conductivity, improved the electrochemical properties of the composite powder with a  $\text{Li}_4\text{Ti}_5\text{O}_{12}/\text{SnO}_2$  ratio of  $0.4/0.6$ .



**Figure 10.** Rate performances of the  $\text{Li}_4\text{Ti}_5\text{O}_{12}\text{-SnO}_2$  composite powders ( $\text{Li}_4\text{Ti}_5\text{O}_{12}/\text{SnO}_2 : 0.4/0.6$ ).

Fig. 10 showed the rate performances of the composite powder with a  $\text{Li}_4\text{Ti}_5\text{O}_{12}/\text{SnO}_2$  ratio of  $0.4/0.6$ , measured at various charge-and-discharge rates. These were measured to investigate the potential of using this powder in applications requiring high power densities. The initial charge capacities of the composite powder were  $572$ ,  $399$ , and  $303 \text{ mAh g}^{-1}$  at the extremely high charge-and-discharge rates of  $3500$ ,  $7000$ , and  $14000 \text{ mA g}^{-1}$ , respectively. In addition, the composite powder was able to retain  $87\%$ ,  $78\%$ , and  $78\%$  of its initial capacity at charge-and-discharge rates of  $3500$ ,  $7000$ , and  $14000 \text{ mA g}^{-1}$ , respectively, after 50 cycles.

#### 4. CONCLUSIONS

The composite powders prepared by spray pyrolysis and subsequently heat treated at 800°C comprised particles with a spherical shape and a hollow structure, irrespective of their  $\text{Li}_4\text{Ti}_5\text{O}_{12}/\text{SnO}_2$  ratios. The high-resolution TEM and dot-mapping images of the composite powders with  $\text{Li}_4\text{Ti}_5\text{O}_{12}/\text{SnO}_2$  ratios of 0.6/0.4 and 0.4/0.6, i.e., those containing  $\text{Li}_4\text{Ti}_5\text{O}_{12}$  and  $\text{SnO}_2$  in reversed ratios, indicated the presence of distinct  $\text{Li}_4\text{Ti}_5\text{O}_{12}$  and  $\text{SnO}_2$  phases. In the composite powder with a  $\text{Li}_4\text{Ti}_5\text{O}_{12}/\text{SnO}_2$  ratio of 0.6/0.4,  $\text{SnO}_2$  nanocrystals several tens of nanometers in size were uniformly distributed in the  $\text{Li}_4\text{Ti}_5\text{O}_{12}$  matrix. However, in the composite powder with a  $\text{Li}_4\text{Ti}_5\text{O}_{12}/\text{SnO}_2$  ratio of 0.4/0.6, the  $\text{Li}_4\text{Ti}_5\text{O}_{12}$  nanocrystals were uniformly distributed in the  $\text{SnO}_2$  matrix, resulting in an increase in electrical conductivity of the powder. The composite powder ( $\text{Li}_4\text{Ti}_5\text{O}_{12}/\text{SnO}_2 = 0.4/0.6$ ) with high electrical conductivity exhibited high capacities and cyclabilities even at a high charge-and-discharge rate of  $700 \text{ mA g}^{-1}$ . This was because of the uniform mixing of the  $\text{Li}_4\text{Ti}_5\text{O}_{12}$  and  $\text{SnO}_2$  phases in the powder, the pure nature of the two phases, and the unique morphologies of the spherical and hollow particles of the powder.

#### ACKNOWLEDGEMENT

This work was supported by the National Research Foundation of Korea (NRF) grant funded by the Korea government (MEST) (No. 2012R1A2A2A02046367). This research was supported by Basic Science Research Program through the National Research Foundation of Korea (NRF) funded by the Ministry of Education, Science and Technology (2012R1A1B3002382). This work was supported by Seoul R&BD Program (WR090671).

#### References

1. G.X. Wang, K.P. Yan, Z.L. Yu, M.Z. Qu, *J. Appl. Electrochem.*, 40 (2010) 821.
2. X. Li, M.Z. Qu, Y.J. Huai, Z.L. Yu, *Electrochim. Acta*, 55 (2010) 2978.
3. F.X. Wu, X.H. Li, Z.X. Wang, H.J. Guo, Z.J. He, Q. Zhang, X.H. Xiong, P. Yue, *J. Power Sources*, 202 (2012) 374.
4. B. Li, F. Ning, Y.B. He, H. Du, Q.H. Yang, J. Ma, F. Kang, C.T. Hsu, *Int. J. Electrochem. Sci.*, 6 (2011) 3210.
5. S.H. Huang, Z.Y. Wen, J.C. Zhang, Z.H. Gu, X.H. Xu, *Solid State Ionics*, 177 (2006) 851.
6. J. Xie, S.Y. Liu, X.F. Chen, Y.X. Zheng, W.T. Song, G.S. Cao, T.J. Zhu, X.B. Zhao, *Int. J. Electrochem. Sci.*, 6 (2011) 5539.
7. J.H. Wang, N. Du, H. Zhang, J.X. Yu, D. Yang, *J. Phys. Chem. C*, 115 (2011) 11302.
8. X.M. Yin, C.C. Li, M. Zhang, Q.Y. Hao, S. Liu, L.B. Chen, T.H. Wang, *J. Phys. Chem. C*, 114 (2010) 8084.
9. X.W. Lou, M.L. Chang, L.A. Archer, *Adv. Mater.*, 21 (2009) 2536.
10. W.M. Zhang, J.S. Hu, Y.G. Guo, S.F. Zheng, L.S. Zhong, W.G. Song, L.J. Wan, *Adv. Mater.*, 20 (2008) 1160.
11. D.W. Kim, I.S. Hwang, S.J. Kwon, H.Y. Kang, K.S. Park, Y.J. Choi, K.J. Choi, J.G. Park, *Nano Lett.*, 7 (2007) 3041.
12. J.S. Chen, D.Y. Luan, C.M. Li, F.Y.C. Boey, S.Z. Qiao, X.W. Lou, *Chem. Commun.*, 46 (2010) 8252.

13. Y.Y. Wang, Y.J. Hao, Q.Y. Lai, J.Z. Lu, Y.D. Chen, X.Y. Ji, *Ionics*, 14 (2008) 85.
14. L.Z. Xing, Z.Q. He, Z.L. Yin, Q.Y. Chen, *Trans. Nanferrous Met. Soc. China*, 20 (2010) s267.
15. A. Sivashanmugam, S. Gopukumar, R. Thirunakaran, C. Nithya, S. Prema, *Mater. Res. Bull.* 46 (2011) 492.
16. R. Cai, X. Yu, X.Q. Liu, Z. Shao, *J. Power Sources*, 195 (2010) 8244.
17. S.H. Park, C.S. Yoon, S.G. Kang, H.S. Kim, S.I. Moon, Y.K. Sun, *Electrochim. Acta*, 49 (2004) 557.
18. J.D. Atkinson, M.E. Fortunato, S.A. Dastgheib, M. Rostam-Abadi, M.J. Rood, K.S. Suslick, *Carbon*, 49 (2011) 587.
19. Y.J. Hong, S.H. Choi, C.M. Sim, J.K. Lee, Y.C. Kang, *Mater. Res. Bull.*, 47 (2012) 4359.
20. Y.N. Ko, H.Y. Koo, J.H. Kim, J.H. Yi, Y.C. Kang, J.H. Lee, *J. Power Sources*, 196 (2011) 6682.
21. K.M. Yang, Y.J. Hong, S.H. Choi, B.K. Park, Y.C. Kang, *Int. J. Electrochem. Sci.*, 8 (2013) 1026
22. M.M. Rahman, S.L. Chou, C. Zhong, J.Z. Wang, D. Wexler, H.K. Liu, *Solid State Ionics*, 180 (2010) 1646.
23. M.Y. Son, S.H. Choi, J.Y. Yun, H.M. Lee, Y.C. Kang, *Int. J. Electrochem. Sci.*, 8 (2013) 703.
24. A.S. Arico, P. Bruce, B. Scrosati, J.M. Tarascon, W.V. Schalkwijk, *Nature Mater.*, 4 (2005) 366.
25. D. Peramunage, K.M. Abraham, *J. Electrochem. Soc.*, 145 (1998) 2609.
26. M. Winter, J.O. Besenhard, *Electrochim. Acta*, 45 (1999) 31.
27. I.A. Courtney, J.R. Dahn, *J. Electrochem. Soc.*, 144 (1997) 2943.
28. I.A. Courtney, J.R. Dahn, *J. Electrochem. Soc.*, 144 (1997) 2045.
29. C.J. Kim, M.J. Noh, M.S. Choi, J.P. Cho, B.W. Park, *Chem. Mater.*, 17 (2005) 3297.
30. H.S. Kim, J.P. Cho, *J. Mater. Chem.*, 18 (2008) 771.